A Study on the Transfer of GISSMO Material Card Parameters from 2D- to 3D-Discretization

Daniel Sommer[a], Florian Schauwecker[a,b], Peter Middendorf[a]

[a]Institute of Aircraft Design, University of Stuttgart, Germany
[b]Mercedes-Benz AG, Research and Development, Sindelfingen, Germany

Abstract

This study presents basic strategies for transfer of LS-DYNA® material card parameters from 2D- to 3D-discretizaion without extensive recalibration. The responses of a material card, calibrated on two-dimensional shell elements, are shown on single-element tests with different element formulations, on multi-element patches and on coupons. From this, magnitudes of error are ascertained and quick recalibration measures on material model parameters are derived.

An evaluation of the stress-state of typical GISSMO-type specimen in different thicknesses and discretization-lengths is given and typical stress-states within the Lode-triaxiality stress-space of these specimens are highlighted. Therefrom, a measure of deviation from the calibrated state can be derived and used as a measure for allowable deviation from the 2D stress-state. Furthermore, the information on the three-dimensional stress-states, even in thin specimen, can be used for quick recalibration of parameters on the failure surface.

Introduction

Many publications on the calibration of material models, especially those focused on *MAT_024 with the GISSMO damage and failure model, employ a two-dimensional discretization of the test specimens, e.g. for steel in [1–3]. Within the industry, this discretization with shells is widely state-of-the art. Thus, the resulting material cards (i.e. the set of parameters for a material model which best represents test data) is calibrated, valid and predictive for a specific shell element formulation [4]. Full 3D Calibration on solid elements are to be found in publications from general material modelling perspectives [5] or for specific, detailed studies [6]. It is however seldom adopted in the industry or even in academia, as it requires extensive testing and tedious work for calibrating the required parameters. For that reason, a 2D-calibrated material card is often directly used in a 3D-discretized analysis, as the engineer has neither time at hand nor data for 3D-calibration available.

With this paper, a study focused on metals is presented, with the aim to give a) more confidence to the use of 2D-calibrated material cards in volumetric models, b) show straightforward methods for quick adaption for 3D analysis and c) examine common GISSMO-type specimen for their stress state in different thicknesses.

The Basics

Elements in Finite Element Analysis:
The dominant discretization method in computational structural mechanics is by finite elements - with their basic concept of subdividing the domain of bodies, loads and supports into simple, calculable elements of a finite number. This enables computation with a finite number of degrees of freedom (DOF), for which a variety of methods for spatial discretization are available. From simplified and abstract modelling to a full three-dimensional representation of real-world bodies, the model and mesh have to be chosen according to different factors, which in the end come down to the engineering judgement of the CAE-engineer. At disposal for geometrical discretization are, from a modelling perspective, the simplest 1D elements like beam and truss or discrete elements such as a spring or damper. They connect only two nodes together with a set of rules given by the element formulation. These 1D elements can represent different bars, beams or pipes, while the finite element idealization

stays the same. Thus, the element formulation must additionally be provided with the cross-sectional area and torsional constants of the real body. Two-dimensional elements connect three or more nodes together to form one shell or membrane element, where the third dimension is only given implicitly through the *SECTION card and considered depending on the element formulation. Finally, three-dimensional elements are made up out of a minimum of five nodes for tetrahedrons or eight nodes for a cubic representation.

In this paper, elements of the shell, t-shell and solid type with different formulations are examined within LS-DYNA with a focus on their response and their limits.

The designated use of shell elements is in parts where the thickness is significantly smaller than the other dimensions of the part: thin parts of the chassis, containers or casings for batteries for example. The real part is discretized at a reference surface from which thickness is defined through the definition in the keyword of the corresponding section. Shell elements are effective and can reduce time for computation, their underlying theory however only allows a plane stress response. All through-thickness stresses are neglected and are not calculated, i.e. $\sigma_{zz} = 0$; a loading from top or bottom of the element is not possible and cross-sections through the thickness remain straight. In this publication shell element type 2 and 16 are used, which are based on Reissner-Mindlin theory [7], where shear deformations are possible. The shell's deformations are described only by the deformation of the reference-surface and its rotation. Elements can generally be categorized by their formulation and their discretization. Type 2 and 16 shells are so-called thin-thin shells: both formulation and discretization are thin, i.e. two dimensional. Type 2 is an under-integrated formulation with only one integration point on the reference surface, where stresses are calculated. It is 2-3x faster than type 16 with 4 integration points, but is also prone to hourglassing modes, which type 16 cannot exhibit. A detailed look on shell theory gives [8], a good overview on elements specifically for LS-DYNA is presented in [9].

Another shell-like element are the thin-thick shells, which have a three-dimensional discretization, but are based on Reissner-Mindlin kinematics. The constitutive law is thus again limited to plane stress but has advantages when transverse shear and bending is investigated. They exhibit no observable locking problems. These shells can be accessed via *SECTION_TSHELL by choosing ELFORM 1 or 2, which are under integrated and fully integrated respectively.

To enable calculation of deformations in thickness direction, a thick-thin shell is implemented and enables a loading of the shell surface with a thickness stretch and a continuous thickness progression. This requires a three dimensional, i.e. thick material description, while the representation stays flat. These shells are therefore called thick-thin shells and are included in part of the studies here. Type 26 is chosen to represent this class in this paper as it based on the robust, often-used type 16 from *SECTION_SHELL.

Another step towards a fully formulated solid-element is a thick-thick shell, as implemented in *SECTION_TSHELL type 3 and 4, which are under- and fully integrated respectively. They have a volumetric discretization and the constitutive formulation is three-dimensional. In contrast to solid elements, it is implemented with respect to efficiency based on a co-rotational implementation of shell type 2, specifically suited for thicker shells with large deformations while locking phenomena are suppressed. They can have multiple through-thickness integration points, whereas solid elements have a maximum of two and have to be stacked. [10]

Following this are finally the solid elements with a complete three-dimensional formulation and discretization, where no reduction and simplification from shell theory is used. In this paper *SECTION_SOLID types 1, an under-integrated formulation with a constant stress approach and type 2, a selective-reduced (S/R) integrated formulation is considered. The former is rather efficient and is suitable for large strains, the latter however requires no hourglass control. This paper in part also considers the modifications in types -1 and -2, which result in an improvement of accuracy with an elongated runtime. [10]

The following Table 1 gives an overview on the most important features and descriptors of the elements used here. For further reading, [10] provides a detailed look into the formulations, while [9] and [11] shall be recommended for an overview suitable for LS-DYNA-specific engineering purposes. Timings in Table 1 are the *Clock(seconds)* timing as per d3hsp from a single element in tension of same size and thickness for a *MAT_024 without failure and same displacement, normalized to shell 16 as the reference. T_{elem} is the clock time used for

element processing and indicates a rising computational time for thicker discretization and formulation. It also shows that seldom used, special element formulations, e.g. T-shell 3 or solid -2 are slower due to a more complex formulation or might not be tuned for speed. The total clock time T_{total} is however not as severely affected, as the element processing is only a part of the complete simulation. However, for runs with more elements, the ratio will increase.

Table 1: Overview of investigated element formulations with characteristic features

	Shell			**T-Shell**				**Solid**			
	2	**16**	**26**	**1**	**2**	**3**	**5**	**1**	**2**	**-1**	**-2**
Formulation	thin	thin	thick	thin	thin	thick	thick	thick	thick	thick	thick
Discretization	thin	thin	thin	thick	thick	thick	thick	thick	thick	thick	thick
Integration	under	full	full	under	full	under	full	under	S/R	under	S/R
T_{elem}	0.46	1	1.7	5.7	9.7	37.6	3.6	3.7	8.0	9	19.4
T_{total}	1	1	1.02	1.56	1.71	2.88	1.51	1.65	1.84	1.85	2.25

Describing the Stress State

It would be bulky to use tensor notation with six components to describe stress and strain states of the elements in the following investigations. Using the three principal stresses $(\sigma_1, \sigma_2, \sigma_3)$, i.e. the Haigh-Westergaard space, is a way of representing the stress state. The basis is the space of principal stresses, in which each stress state can be represented. In this space, a cylindrical coordinate system (z, r, Θ) can be denoted and is useful for easy representation of stress state:

The z-axis is defined where principal stresses are equal, i.e. $\sigma_1 = \sigma_2 = \sigma_3$, it thus indicates the hydrostatic component and is defined as

$$z = \sqrt{3}\,\sigma_m = \frac{I_1}{\sqrt{3}}. \tag{1}$$

where I_1 is the first stress invariant and σ_m is the mean hydrostatic stress defined by

$$\sigma_m = \frac{1}{3}(\sigma_1 + \sigma_2 + \sigma_3). \tag{2}$$

The r coordinate corresponds to the magnitude of the deviatory component, which can be described by means of equivalent stress:

$$r = \sqrt{2/3}\,\sigma_{eq} = \sqrt{2J_2}. \tag{3}$$

Where J_2 is the second independent deviatory invariant and σ_{eq} is the von Mises- or equivalent stress:

$$\sigma_{eq} = \frac{1}{\sqrt{2}}\sqrt{(\sigma_1 - \sigma_2)^2 + (\sigma_2 - \sigma_3)^2 + (\sigma_3 - \sigma_1)^2} = \sqrt{3J_2}. \tag{4}$$

The last spacial coordinate Θ is the Lode angle. It fully defines the stress state on the deviatoric plane spanned by z and r. The origin of the angle is defined in the context of LS-DYNA by

$$\Theta = \frac{1}{3}\arccos\left(\frac{J_3}{2}\left(\frac{3}{J_2}\right)^{\frac{3}{2}}\right), \tag{5}$$

but can be found in literature defined by positive and negative sine or tangens. Handier than this bulky formulation is using the Lode parameter ξ instead of the angle Θ. It is defined by:

$$\xi = \cos(3\Theta) = \frac{J_3}{2}\left(\frac{3}{J_2}\right)^{\frac{3}{2}} = \frac{27}{2}\frac{J_3}{\sigma_{eq}^3}, \tag{6}$$

which is a normalization of the third deviatoric invariant using equivalent stress. The possible range of ξ is between -1 and 1.

The important idea to take away from this is, that everything in this cylindrical system can be expressed by z, r, ξ which is derived from the invariants J_2, J_3, I_1 or from σ_m, σ_{eq} and J_3. With these, the stress state at a material point can be exactly defined. For a characteristic stress state however the magnitude can be disregarded – a tensile stress state for example will be tensile no matter the magnitude – only two independent variables are needed: the

Lode-parameter ξ and the triaxiality η, a dimensionless pressure defined as the ratio of mean, hydrostatic pressure and von Mises stress:

$$\eta = \frac{\sigma_m}{\sigma_{eq}} = \frac{1}{3\sqrt{3}} \frac{I_1}{\sqrt{J_2}} \tag{7}$$

More importantly, the afore introduced shells with a thin constitutive formulation, can only represent a stress state of plane stress. For this two-dimensional loading, only one of the two parameters are needed, as they are connected by the following relation for plane stress [12]:

$$\xi = -\frac{27}{2}\eta(\eta^2 - \frac{1}{3}) \tag{8}$$

Here, the Lode parameter ξ can be expressed using η, which thus remains as the sole variable for description of a plane stress state (without its magnitude) for shell formulations.
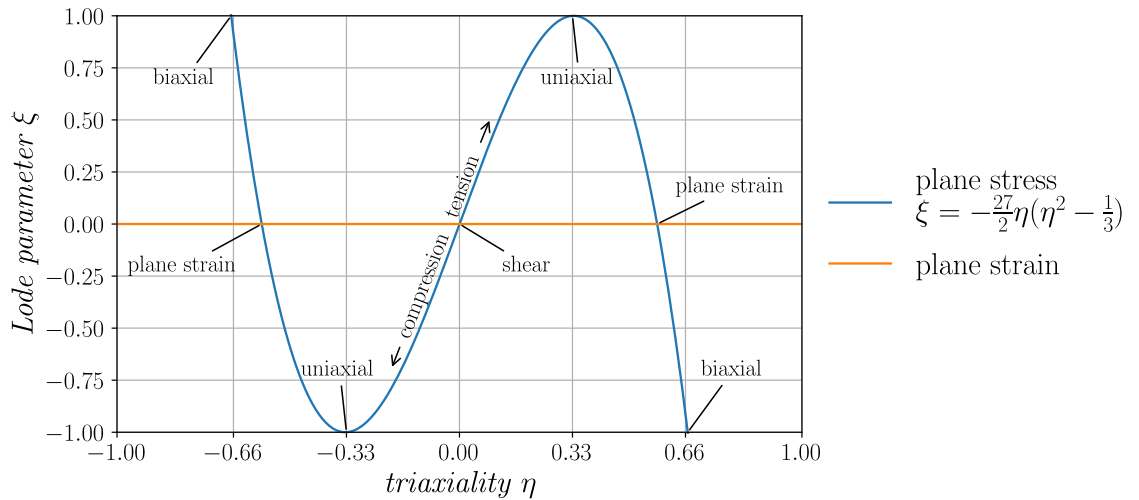

Figure 1: Characteristic stress states in the 2D triaxiality-Lode-parameter-plane.

From Figure 1 becomes clear that many stress states cannot be represented by thin-formulated shell elements, as the possible states are located only on the blue plane stress curve, whereas a three-dimensional stress state can take any value of ξ or η. The possible range of η for a plane stress state is $-\frac{2}{3} < \eta < \frac{2}{3}$, as the quotient of σ_m and σ_{eq} cannot yield any other value when $\sigma_3 = 0$. For three-dimensional stress the Range is $\mathbb{R}$ - all real numbers. Whereas ξ is always ranged between -1 and 1 for both two- and three-dimensional states. Table 2 gives values of triaxiality and Lode parameter for characteristic stress states in the plane stress domain, where again, one of the two values would be enough to describe it.

Table 2: Values of triaxiality and Lode parameter for characteristic 2D stress states (after [13])

Loading		Triaxiality η	Lode parameter ξ
	biaxial compression	2/3	1
	plane strain compression	$-\sqrt{3}/3$	0
	uniaxial compression	-1/3	-1
	torsion/pure shear	0	0
	uniaxial tension	1/3	1
	plane strain tension	$\sqrt{3}/3$	0
	biaxial tension	2/3	-1

A very Brief Introduction to Material Models in LS-DYNA

The constitutive formulation couples strains to stresses and needs to be evaluated for each element, as mentioned before. As of Version R11, LS-DYNA has material numbers up to 296, with additional options and features that can be added to each material model. This highlights the vast options to model materials within the software. Of course, many models have very specific purposes, for different classes of materials or special use-cases. In the scope of this contribution, material models suitable for metals are used for the investigations, specifically *MAT_PIECEWISE_LINEAR_PLASTICITY or *MAT_024 and the additional failure and damage model *MAT_ADD_DAMAGE_GISSMO.

Some elasto-plastic material models are implemented, of which *MAT_024 is probably the best known. This model behaves elastically until the von Mises yield condition is fulfilled. It states that the flow behaviour is influenced by the shape changing component of the stress tensor only, i.e. it is independent of hydrostatic stress σ_m. Thus, plastic flow occurs when σ_{eq} (see eq.(4)) exceeds a user-defined defined limit value. Afterwards, the solver takes a tabulated input of corresponding plastic strains ϵ_{pl} and equivalent stresses σ_{eq} to model the plasticity flow curve. Since this model does not consider any accumulation of damage, the failure is abrupt at a given maximum plastic strain. *MAT_024 provides a convenient straightforward way of modelling materials with a distinct plastic behaviour and is oftentimes considered the "workhorse" of material models in LS-DYNA. When materials, like metals, exhibit a much more complex stress-strain response, for example a different plastic flow response for different stress states or an anisotropic behaviour, this model reaches its limits.

There are a few material models which extend *MAT_024. Some, e.g. *MAT_089 or *MAT_187 add strain rate dependent failure and add more flexibility in damage and failure modelling. Others offer even more flexibility, e.g. *MAT_224, which can model failure strain dependent on triaxiality, i.e. the stress state [14]. However, the greatest flexibility offers the phenomenological *MAT_ADD_EROSION with IDAM=1, or in versions from R11, *MAT_ADD_DAMAGE_GISSMO [4, 15]. With this "Generalized Incremental Stress State dependent damage Model" (GISSMO) all other implemented damage and failure approaches can be modelled. It can for example be used to remodel a Johnson-Cook behaviour from *MAT_224. The charm is, that it provides full flexibility on the modelling of damage and failure as it offers many features for user-defined control and can be added to any base material model having plasticity. Its flexibility is only surpassed by *MAT_ADD_GENERALIZED_DAMAGE [16], which comes with even more tuneable parameters on anisotropy. Using GISSMO, the user gets the ability to add the following main features to any material model:

- stress-state, temperature and strain-rate dependent plastic failure strain: $\epsilon_{pl,fail}(\xi, \eta, T, \dot{\epsilon})$,
- custom accumulation of damage, dependent on strain path: $D = (\epsilon_{pl}/\epsilon_{pl,fail})^n$
- custom coupling of damage to stress to introduce softening effects at a custom plastic strain onset
- element-size specific failure strains and softening exponents, i.e. so-called regularization.

With these features, it can provide exceptional results compared to those cards using a no damage modelling or a conventional damage modelling approach [4]. When modelling metallic components with great attention to detail, especially for high-dynamic crash loadings there is almost no way around this model. However, this flexibility requires an appropriate calibration and validation of nine parameters, three of them defined as functions and not only as scalar values. In order to capture a full three dimensional stress state, the failure curve even extends to a surface, adding additional parameters [5]. The corresponding parameter identification becomes a non-trivial task resulting in tedious work for the manual analytical approach.

For characterization of a material to be fully described by a GISSMO model, a set of specimens have been established to find the best set of parameters by reverse-engineering. For calibration of a shell model the commonly used specimens are described in [4] with exact dimensions and drawings for reproduction. As outlined there, they are the common ground of specimens from several contributions. They can be distinguished into three categories: Small specimen with dimensions of 20 mm width and 60 to 80 mm length with different geometries for characterization of multiple stress states. These are: small tensile test for triaxialities starting at 0.33 before necking, notched tensile and shear 45° for slightly higher triaxialities between 0.4 and 0.5 and shear 0° for

triaxialities near 0. Secondly, the large tensile test similar to DIN EN ISO 6892 with a strain gauge of 80 mm and thirdly a deep-drawing-test for a biaxial loading like the Nakajima or Bulge test [4]. The small specimens are used, as outlined, for calibrating most parameters of the model: critical and failure plastic strain curves, softening parameters and strain-rate dependence if needed. These specimens require a fine discretization, as load-carrying sections are around 5 mm. To capture effects like localization after necking, a mesh size around 0.5 mm is required. As full-scale simulations of parts or assemblies are discretized with elements 10 times larger, a transfer to these sizes must be made. Elements of these scales cannot discretize the geometry of the small specimen anymore, thus the A80 specimen is used for upscaling. But as the large elements cannot represent the effects like localization after necking in metals, as their dimension is much larger than the size of the effect they shall represent, a technique called regularization is employed. Model parameters are coupled to element size with scaling factors, so that larger element sizes represent the global behaviour of the component, such as localization or crack formation, even if they do not deliver the correct local prognosis. For GISSMO this is the plastic strain to failure vs. triaxiality curve and the softening vs. triaxiality curve, which can and have to be scaled depending on element size. These parameters have then no longer physical coupling to measured values and are completely phenomenological, but the model is still able to globally consider effects smaller than element length.

To calibrate the GISSMO model for a three-dimensional stress-state, parameters can be described with a lode-angle dependence, e.g. the plastic strain to failure or the onset of necking. In this case the failure curve $(\epsilon_{pl,fail}, \eta)$ will turn into a surface and is described by multiple failure curves $(\epsilon_{pl,fail}, \eta)$ for different Lode-parameters Θ. To test for lode angle dependence, [5] developed a set of specimens which exhibit a specific three dimensional stress state away from plane stress. These specimens are very detailed, must be discretized very finely and are difficult to manufacture. Thus, we will now have a look on transferring a two-dimensional calibration to a three dimensional without no or few extra testing.

Response of the Model in Shell and Solid Elements

The following investigates the response of a 2D-calibrated GISSMO model for a generic metal on shell, T-shell and solid elements. At first the response of a single element subjected to different loadings to show the responses on element-level, in a second step a rectangular patch made of a limited number of elements is analysed. Results have been validated using four separate material cards: two for steel, complex and dual-phase and two for different aluminiums. As results discussed here are independent of magnitudes of stress or strain, they will be shown qualitatively normalized to the baseline SHL16. All material cards were calibrated using shell discretization on the tests introduced in the previous section and regularized for an element-range between 0.5 mm and 10 mm.

Single-Element Responses
The numerical simulation in this section is limited to single elements under tensile, compressive and shear loads. With this, there are no interactions between adjacent elements, the strain path is controllable, and the post-processing is significantly simpler. A single element test is generally used to verify and analyse the behaviour of the material model with the calibrated values. The influences of the input parameters on the stress-strain response can be checked and potential flaws eliminated on this level. In the crash simulation, grid coarseness in the order of 3 to 5 mm are currently used. Therefore, rectangular elements with sizes of 0.5 mm, 1 mm, 2.5 mm, 3 mm, 5 mm, 8 mm and 10 mm were simulated here.

Figure 2 shows the results of two different configurations: thin elements with a thickness of 1 mm for all sizes. On the right all elements are cubic, i.e. thickness is equal the element edge length. Stress is shown normalized to the maximum stress of shell formulation 16. The figure includes shell formulations 1,2 and 16; solid formulations -2, -1, 1, 2 and thick shell formulations 1 and 2. Shell formulation 26 (thick-thin) is not plotted, as it follows the progression of the thin-thin shells at first and then diverges towards the solid progression of corresponding size. Thick shell formulation 3 is also not shown, as is has an erroneous progression after the onset of necking. Both of which might be avoided by further parameter tweaking but shall not be the focus here.

The different behaviour of the different sizes results from regularization, which was introduced in the previous chapter, and enables the correct response of a specimen or part when discretized with large elements. Shell formulations show no change in response, no matter the thickness, as they have only a virtual thickness. Element size for regularization is calculated by $l_{element} = \sqrt{l_1 l_2}$, where l_1 and l_2 are the length of the two axis of the element.

Solid formulations give the same response as shell elements only when they are cubical. For non-cubic (i.e. flat or thick) elements, they give a different response with slower damage and higher failure strains (see Figure 2, left). This is again attributed to the calculation of the calculated element size $l_{element}$, which is equal to $\sqrt[3]{l_1 l_2 l_3}$. With this, wrong regularization factors are used for scaling of the plastic strain to failure and the fade-exponent, which leads to a different answer of a solid element compared to the calibrated shell element, when it is not cubic.
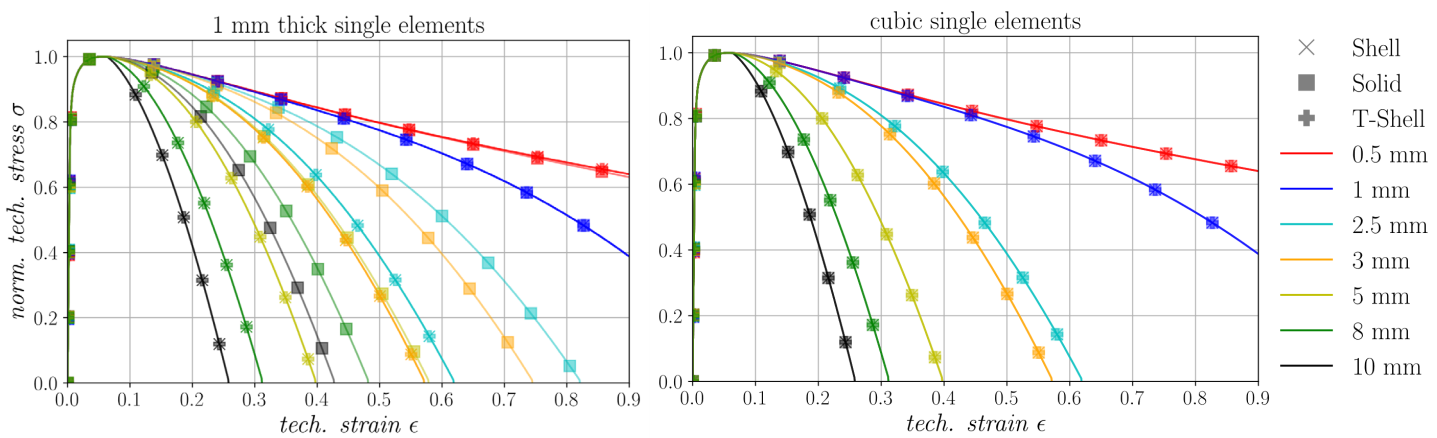

Figure 2: Comparison of single-element of different size (0.5 - 10 mm) tensile response of a generic material card. Left: response of 1 mm thick elements; Right: response of cubic single elements

The same behaviour is observed for other stress states than tension with the exception when SHRF or BIAXF are set near 1 or -1 in the material card. This disables regularization for shear or biaxial stress state or at the intersection of the failure curve with the instability curve respectively and does thus not present this effect for these states.

To match the response of the solid element to the calibrated response of the shell elements, regularization must be adapted, so that the calculated element size of the solids is matched with the regularization factors determined for the shell element sizes. For example, a 4 x 4 x 2 mm shell would have an $l_{element}$ of 4 mm, whereas the element size of a solid of same dimension would yield 3.175 mm. The tables in the material card have thus to be updated depending on element thickness of the solid – only then solids yield the same results as the calibration.

Another important factor is ISTUPD, which shall be discussed very briefly. This parameter in *CONTROL_SHELL is determining if a thickness update is considered in deformable shells. Figure 2 shows results for ISTUPD=3, as with this setting all elements give same results for the cubic case and for the thin elements t-shells 1&2 even give the same result as shells. This setting causes a change in the thickness, when the elements are membrane strained, which is important for the stress response as the load-carrying area changes. Setting ISTUPD to 0, thickness changes are not calculated, which makes thin formulations respond with a higher maximum stress, while keeping the correct failure strain. This results in an overestimation of maximum internal energy to failure. Setting ISTUPD=4 is recommended for crash analysis [14] and uses only plastic strains for calculation of the thickness change, which makes the shell formulations (1,2,16) respond as the solids do. But thick shells (1&2) do still respond with a higher energy. ISTUPD=3 chooses the 'correct' update for both shell and t-shells, using ISTUPD=1 for shell elements and ISTUPD=2 for thick shells. The correct ISTUPD shall thus be set for the correct element type to give the calibrated response.

Behaviour of Multiple Elements in a Patch

A structure will be represented by more than only one element in most cases. A step towards a coupon specimen is a patch of elements, where a rectangular patch made up of several elements is subjected to defined loading. Using the material models with the adapted, fitting regularization, a patch with dimensions 30 x 30 mm² was subjected to a tensile loading (see Figure 3, left top). It was discretized by shells and t-shells of thickness 3 mm, as well as with three solids over the thickness. Compared to the single-element test, the load path of the elements does now change over the course of loading, in contrast to the single element test, where the stress state stays constant over the simulation. Elements in the middle of a patch in tension will be subjected to a more complex stress state, as neighbouring elements now have an influence on each other and the whole coupon will contract, resulting in a biaxial stress state in the centre elements (see Figure 3, left bottom).

The different element formulations, while showing same behaviour in a single element test, now exhibit a differing response in the patch. In the elastic region responses are exactly alike as expected, whereas maximum stress and failure strain can differ. To be able to compare the different element sizes and formulations, Figure 3, right compares the maximum internal energy of the patches until failure. This represents the area under the stress-strain-curve, i.e. higher stresses and/or higher strains to failure will lead to a higher internal energy. The energy has been normalized by the maximum internal energy of shell 16 with 1 mm element length, as only a qualitative comparison is needed here.
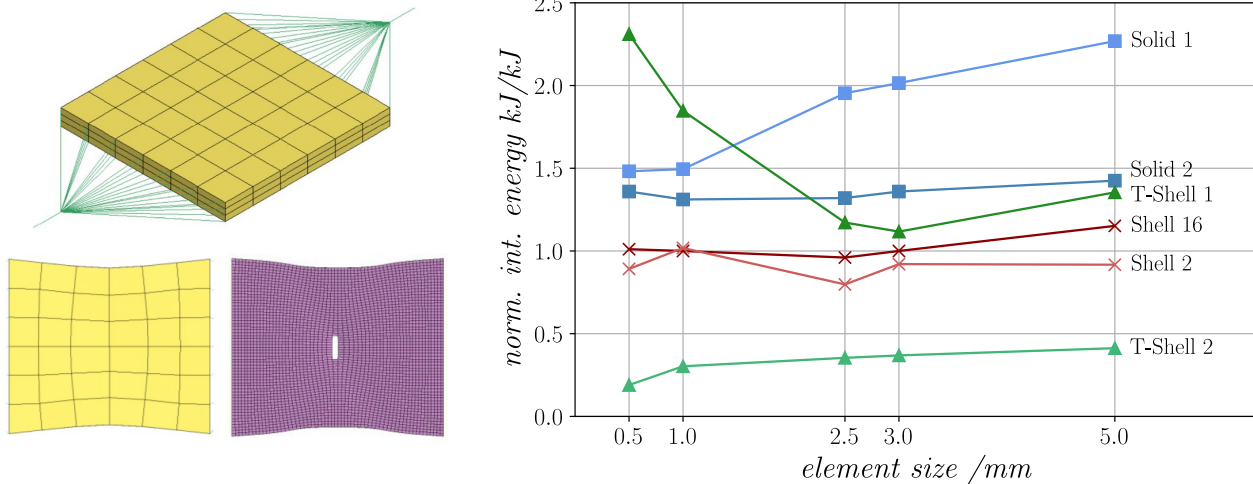

Figure 3: Right: Normalized maximum internal energy (to shell 16, 1.0 mm) vs. element size for patches of different element types and sizes; Left, top: Solid coupon, 5mm with load introducing beams in green; Left, bottom: 5 mm and 0.5 mm (lilac) patch at same displacement.

Figure 3,right gives insights into the response of the different formulations: The fully integrated shell 16, which shall be the baseline, shows a response independent of element size, the standard deviation is only 0.065 kJ/kJ, with a 5 mm element size however responding 14% stiffer than 1 mm. It indicates regularization is successfully accomplished and calibrated in this material card for shell 16 but might be tweaked for larger element sizes. Both shell formulations, under integrated (2) and fully integrated (16) are on average 10% apart, with the under integrated patches being lower and for 2.5 mm the lowest with 20% more compliance. Shell 2 give a slightly more divergent response to element size; its standard deviation is 0.07 kJ/kJ. The selective-reduced integrated solid formulation type 2 is on average 34% stiffer than shell 16, with a low standard deviation of 0.04 within the formulation in this range of element sizes. The under integrated solid formulation type 1 has a much more divergent behaviour (std. dev.: 0.3) and stiffens with element size. Its mean difference from shell 16 is 82 %. The most extreme values are reached with thin-thick shell formulation 1, where stiffening occurs, contrary to solid 1, with smaller element sizes. Its mean divergence by 52% from shell 16 is both large and misleading, as it shows very low deviation at sizes around 3 mm (10% dev.) but is very high for 0.5 mm (129% dev.). This is reflected in the standard deviation of 0.45 for t-shell 1. The thin-thick formulation 2 is the most compliant with only 32% of

the stiffness of shell 16 on average. Standard deviation of 0.07 kJ/kJ shows however good independence of element size, which could promise good results when recalibrating specifically for this formulation.

Transferring 2D-calibrations to 3D

The method of adapting the regularization for solid formulations is a very convenient and quick method to get the same answer from a material card as shell formulations would give. This means, the calibration will still be valid if - and most certainly only if - the stress state stays close to the plain stress state. For thicker parts, the failure surface can be constructed by using additional test geometries which produce a stress state further away from plane stress. These can be for example specimens as introduced by Basaran [5]. Furthermore, assumptions on how the 2D failure curve can be used to construct a 3D failure surface analytically, without further testing, have been used by Bai and Wierzbicki [13]. Here, three failure curves for distinct lode-parameters, as suggested in [17], are connected by a quadratic formulation to generate a failure surface. This has been adapted in Schauwecker et.al. [6], where additional assumptions or failure under large pressure triaxialities were made. Tests from plane-strain specimens [4] or three-dimensional specimens [5] can be used as support points for fitting analytical formulations or fitting a mathematical representation of bi-splines, as shown in [5]. These methods (auto-adaption of regularization, analytical method for fracture locus description as well as mathematical bi-spline best fit) have been implemented to transfer 2D cards automatically for solid formulations. Underlying are however assumptions on the failure surface for untested stress states and may lead to a false representation for these stress states. To check, it is best to determine how far apart the stress states in the final part are from stress states used for calibration and use fair judgement on how dependable the fracture points are.

The characteristic deviation k from plane stress shall be introduced here. The distance of the stress state from the corresponding plane stress state can be used:

$$k = |\sigma_{2D} - \sigma_{3D}| \tag{9}$$

where

$$\sigma_{2D} = \begin{pmatrix} \eta \\ -\frac{27}{2}\eta\left(\eta^2 - \frac{1}{3}\right) \end{pmatrix} \quad ; \quad \sigma_{3D} = \begin{pmatrix} \eta \\ \xi \end{pmatrix} \tag{10}$$

is the plane strain stress state determined by the current triaxiality and the fully three-dimensional stress state respectively.

A closer look at the stress state in GISSMO-style specimen

The specimens, as summarized in [4], are used for 2D-calibration normally, i.e. the specimens are discretized using shell elements. A closer look on the stress state using simulations of these specimen shall now reveal possibilities in using these 2D specimen for a description of a 3D failure surface. The focus is the A80, mini-tension (MT) and notched-tension (NT) specimens, which have been simulated with varying thicknesses, whereas the rest of the geometry has been kept original. To be able to represent the geometries, a dimensionless thickness β is introduced, which is the thickness t normalized by the width w of the load-carrying part of the specimen.

$$\beta = \frac{t}{w} \tag{11}$$

To be able to evaluate the stress state at different points in the specimen, up to seven different sets of elements in the load-carrying cross-section of the specimen have been selected and their properties are evaluated. If a set is made up of more than one element, values must be averaged. For the averaging of sets and for determining global averages of the properties, the same weighting function g as for damage accumulation within the GISSMO model [4] is used:

$$g = \frac{n}{\epsilon_{pl,fail}^{n}} \epsilon_{pl}^{n-1} = \frac{n}{\epsilon_{pl,fail}} D^{\frac{n-1}{n}} \tag{12}$$

Where n is the damage exponent as set in the material card, $\epsilon_{pl,fail}$ the plastic strain to failure for the current stress state, as defined by the failure curve/surface $\epsilon_{pl,fail}(\xi, \eta, T, \dot{\epsilon})$ and D is the current Damage. The weighting of any variable x, e.g. η or θ, is then obtained by

$$\bar{x} = \frac{1}{\mu} \sum_{i=1}^{I} g_i x_i \tag{13}$$

Where i and I is the current and final timestep respectively or current and number of elements respectively and μ is the sum of the weighting function:

$$\mu = \sum_{i=1}^{I} g_i \tag{14}$$

In a first study, the element size is kept constant for different thicknesses, i.e. the tests as shown in Table 3 are simulated with varying number of elements of size 0.5 mm through thickness. Figure 4 shows the cross section of the load-bearing part of the mini tension (MT) specimen for different dimensionless thicknesses with element size of 0.5 mm and coloured element sets for evaluation. A80 and notched tension (NT) are partitioned similarly.

Table 3: Simulated configurations with constant elementation of 0.5 mm for different thickness-width-ratios

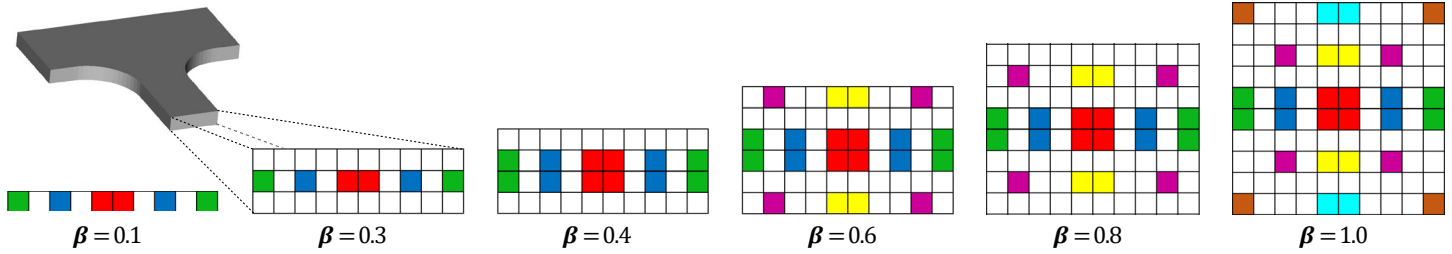| A80 β	0.05	0.15	0.2	0.4	0.6	0.8	1
A80 no. elements	1	3	4	8	12	16	20
Mini-/notched tensile β	0.1	0.3	0.4	0.6	0.8	1	
MT/NT no. elements	1	3	4	6	8	10	

Figure 4: Evaluated sets for different thicknesses; here: for the mini tension (MT) specimen.

For these specimen the average values of triaxiality and Lode parameter, weighted by the GISSMO weighting function (12), of all elements in the sets are plotted for the mini tension specimen in Figure 5. From left to right, the thickness of the specimen increases from $\beta = 0.1$, i.e. 0.5 mm to $\beta=1$, i.e. 5 mm. Specimen were simulated with fully integrated solid elements 2. The regularization in the material card has been adapted. The mean weighted values of the set over the plastic domain are marked with a ◆ and final failure of the first element in the set with ×. Due to the constant element size in this setup with a constant cubic element size of 0.5 mm, the number of sets grows with rising β.
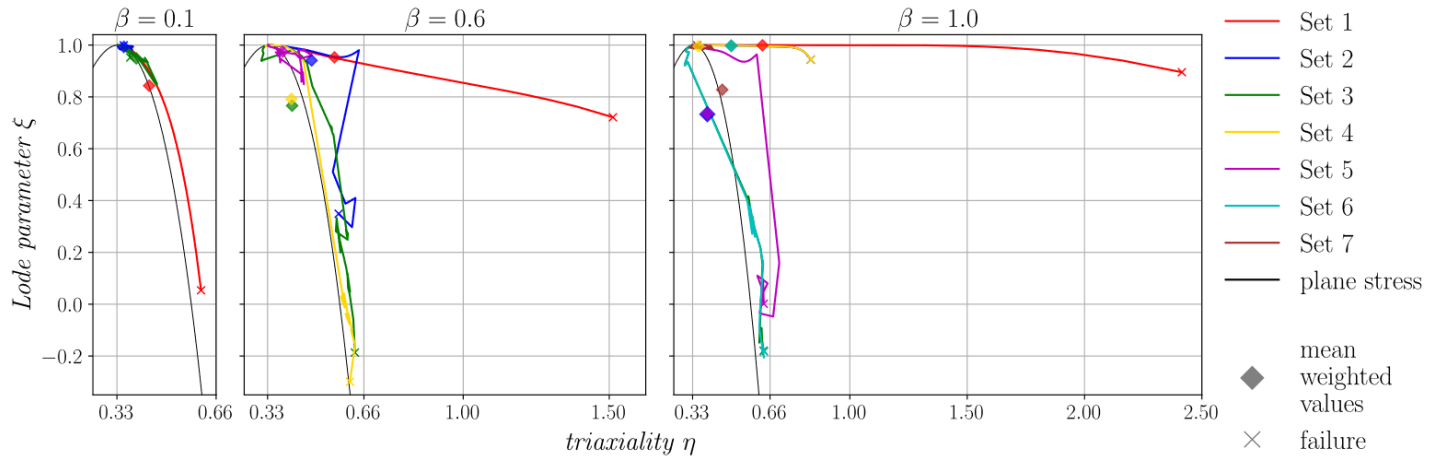
Figure 5: Stress states for mini tensile specimen from β=0.1, 0.3 and 1 of the sets from Figure 4.

The growing three-dimensionality, i.e. deviation from plain stress (marked black in Figure 5), with rising ratio of thickness/width becomes apparent. While for thin specimen, the stress state is close to the plane stress state, as they were designed by [4], the distance from the 2D stress state grows with rising aspect ratio β and plastic strain ϵ_{pl}. For β=0.1 the mean weighted values are on the plane stress curve, for β=1, they have migrated towards a three-dimensional state. The mean weighted values of triaxiality and Lode parameter are closer to the plane stress state than the point of failure, as for most of the virtual test, the stress state is closer to the plane stress state – only for higher plastic strains, they diverge. Large jumps in the progression of the curves result from other failing elements, which results in a shift of the flux of force and a change in loading, i.e. stress state.

When discretizing the thin specimen with smaller elements the evaluation of all seven sets as in Figure 4, right is possible. In this configuration all seven sets yield a stress state close to the plane stress. The fine resolution i.e. gives a more detailed look into the thin specimen and reveals stress states within the boundaries set by coarser discretization. The observed effects in Figure 5 and Figure 6 are thus not from rising element quantity and better resolution, but can be attributed to the rising thickness.

This observation is valid for all specimens under investigation here: the mini tensile, the A80, the notched tensile specimen. Figure 6 shows average triaxialities vs. average Lode parameter for each set from all specimen from Table 3. The rising three-dimensionality becomes even more clear from this. The thick specimen cover the region as axisymmetric notched round specimen from [5]. Additionally, each of the three specimens occupy a specific region in the stress state space.
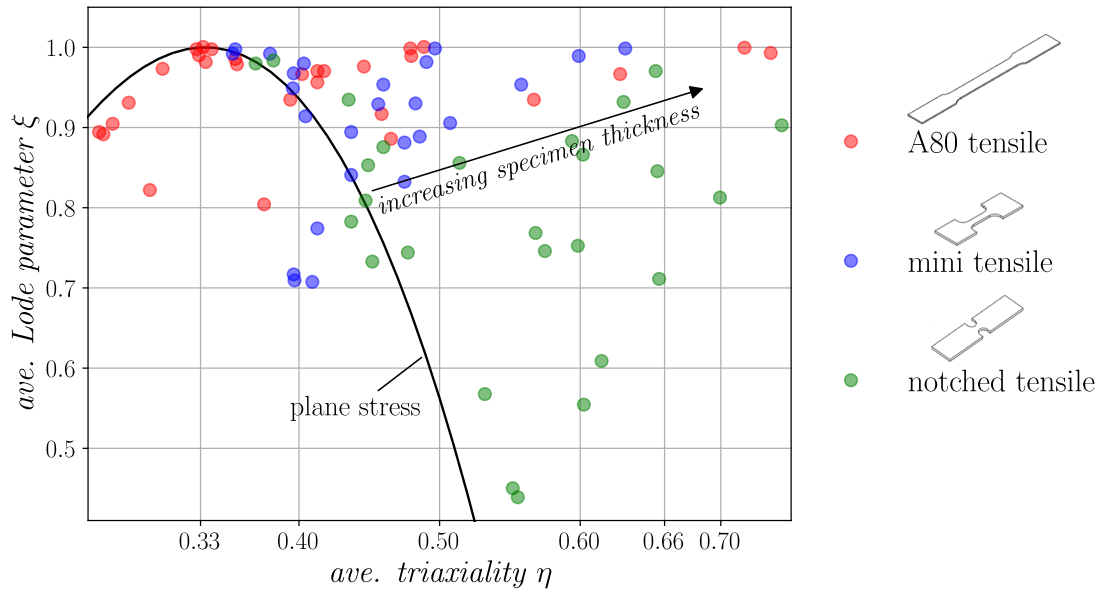
Figure 6: Found average triaxialities vs. average Lode parameters for shown specimen from β=0.5-1 of all sets from Figure 4.

Conclusion

To conclude this small study, an automated adaption of the 2D regularization from shells to the new solid thickness can be recommended as the least action to use two-dimensional material cards with thick formulations. It provides a quick and straightforward measure to make the answer of the card closer to the calibrated results for solids.

The analysis of multiple elements in a patch provides a method to check thin and thick formulations and can be used for a recalibration of GISSMO parameters by tuning the parameters, best by means of an optimization. This enables an even better agreement of response of both dimensions and highlights possible erroneous energy answers of specific formulations and helps to choose appropriate element formulations for part analysis.

When no specific testing with dedicated specimens exhibiting a three-dimensional stress state is undertaken, the presented analysis gives the three-dimensional stress states for 2D-geometries, which can be used as points for construction of the 3D failure surface by existing methods. Additionally, it enables the use of well-known, easy to manufacture geometries with larger thicknesses for supplementary fulcrums for the failure surface obtained from one additional test.

Using an unaltered 2D material card for 3D analysis can thus be advised against, the least measures to be automated is to adapt the regularization table to the solid thickness. This could mean more material cards for the same material when different thicknesses are used in a simulation. The generation of analytical/mathematical failure surfaces on three-dimensional stress states of GISSMO-style specimen has also been discussed and automated.

In a next step, as an outlook, the actions for dimensional transfer presented here can be used for analysis on the level of components. This has to be validated with testing of thick parts to show the performance of each of the steps on dimensional transfer outlined here.

References

[1] G. Falkinger and P. Simon, "An Investigation of Modeling Approaches for Material Instability of Aluminum Sheet Metal using the GISSMO-Model," *10th European LS-DYNA Conference*, Würzburg, Germany, 2015.

[2] X. Chen, G. Chen, L. Huang, M. F. Shi, "Calibration of GISSMO Model for Fracture Prediction of A Super High Formable Advanced High Strength Steel," *15th International LS-DYNA Conference 2018*, Detroit, MI, USA, 2015.

[3] A. Trondl, S. Klitschke, W. Böhme, D.-Z. Sun, "Verformungs- und Versagensverhalten von Stählen für den Automobilbau unter crashartiger mehrachsiger Belastung," *FAT-Schriftenreihe*, 283, IV, Berlin, Germany, 2016.

[4] F. X. C. Andrade, M. Feucht, A. Haufe, and F. Neukamm, "An incremental stress state dependent damage model for ductile failure prediction," *Int J Fract*, vol. 200, 1-2, pp. 127–150, 2016.

[5] M. Basaran, *Stress state dependent damage modeling with a focus on the lode angle influence*. Zugl.: Aachen, Techn. Hochsch., Diss., 2011. Aachen: Shaker, 2011.

[6] F. Schauwecker, D. Moncayo, M. Beck, P. Middendorf, "Investigation of the Failure Behavior of Bolted Connections under Crash Loads and a Novel Adaption to an Enhanced Abstracted Bolt Model," *15th International LS-DYNA Conference 2018*, Detroit, MI, USA, 2018.

[7] E. Reissner, "On the theory of transverse bending of elastic plates," *International Journal of Solids and Structures*, vol. 12, no. 8, pp. 545–554, 1976.

[8] D. Chapelle and K.-J. Bathe, *The Finite Element Analysis of Shells: Fundamentals*. Berlin, Heidelberg: Springer-Verlag Berlin Heidelberg, 2011.

[9] A. Haufe, K. Schweizerhof, P. DuBois, "Properties & Limits: Review of Shell Element Formulations," *Developer Forum*, Filderstadt, Germany, 2013.

[10] Livermore Software Technology Corporation, "LS-DYNA Theory Manual," 07/22/17 (r:8697).

[11] T. Erhart, P. Du Bois, and F. X. C. Andrade, "Short Introduction of a New Generalized Damage Model," *11th European LS-DYNA Conference*, Salzburg, Austria, 2017.

[12] T. Wierzbicki and L. Xue, "On the effect of the third invariant of the stress deviator on ductile fracture," *Impact and Crashworthiness Laboratory, Technical Report*, vol. 136, 2005.

[13] Y. Bai and T. Wierzbicki, "A new model of metal plasticity and fracture with pressure and Lode dependence," *International Journal of Plasticity*, vol. 24, no. 6, pp. 1071–1096, 2008.

[14] Livermore Software Technology Corporation, "LS-DYNA Keyword User's Manual Vol II," 10/12/18 (r:10572).

[15] F. Neukamm, *Lokalisierung und Versagen von Blechstrukturen*. Stuttgart: Institut für Baustatik und Baudynamik der Universität Stuttgart, 2018.

[16] T. Erhart, "Review of Solid Element Formulations in LS-DYNA," *LS-DYNA Forum 2011*, Stuttgart, Germany, 2011.

[17] G. R. Johnson and W. H. Cook, "Fracture characteristics of three metals subjected to various strains, strain rates, temperatures and pressures," *Engineering Fracture Mechanics*, vol. 21, no. 1, pp. 31–48, 1985.